RADIATION RESEARCH **160**, 174–185 (2003)
0033-7587/03 $5.00

Electron Spin Resonance Study of DNA Irradiated with an Argon-Ion Beam: Evidence for Formation of Sugar Phosphate Backbone Radicals

David Becker, Amanda Bryant-Friedrich, CherylAnn Trzasko and Michael D. Sevilla[1]

Department of Chemistry, Oakland University, Rochester, Michigan 48309-4477

Becker, D., Bryant-Friedrich, A., Trzasko, C. and Sevilla, M. D. Electron Spin Resonance Study of DNA Irradiated with an Argon-Ion Beam: Evidence for Formation of Sugar Phosphate Backbone Radicals. *Radiat. Res.* 160, 174–185 (2003).

In this study, the effects of high-LET radiation on DNA were investigated and compared with the effects of γ radiation. Hydrated DNA samples at 77 K were irradiated with argon-ion beams (^{36}Ar or ^{40}Ar beam at energies between 60 and 100 MeV/nucleon). The individual free radicals formed were identified and their yields were investigated by electron spin resonance spectroscopy. Argon-ion irradiation resulted in lower yields of base ion radicals and higher yields of neutral radicals than γ irradiation. A hitherto unknown species was assigned to the radical formed by C–O bond rupture at the deoxyribose C3′, resulting in a sugar carbon-centered radical. A previously characterized phosphorus-centered radical was also found. The formation of each of these species was accompanied by an immediate strand break. *G* values, *k* values, and analyses for the individual yields of neutral radicals and ion radical composition for argon-ion-irradiated hydrated DNA are reported and compared to those found previously for γ-irradiated DNA. The lower *G* values and *k* values for ion radicals and the higher fraction of neutral radicals found for argon-ion-irradiated DNA are attributed to differences in track structure inherent in the two radiations.

INTRODUCTION

The processes of energy deposition by heavy ions and the subsequent damage to the DNA within living cells have received considerable attention. However, the study of the chemical events that follow heavy-ion irradiation of DNA itself is still an emerging effort. For direct-type effects (*1*, *2*), which are the sums of the direct and quasi-direct effects (*3*), clear differences between the effect of low-linear energy transfer (LET) radiation on DNA and the higher-LET radiation provided by heavy ions have been reported (*4*, *5*).

First, the *G* values of radicals stabilized in hydrated DNA samples irradiated at low temperatures are lower with high-LET radiation than with γ radiation. In addition, the fraction of neutral radicals in the radical cohort is higher for heavy-ion radiation than for lower-LET radiation. These differences were attributed to the greater recombination of ion radicals (relative to neutral radicals) in the densely ionized heavy-ion track which consequently results in the stabilization of fewer ion radicals in DNA exposed to high-LET radiation than in DNA exposed to low-LET radiation DNA (*4*, *5*). In addition, ESR spectra of samples irradiated with heavy ions show the presence of a phosphorus-centered radical ($ROPO_2^{-\bullet}$) in yields of about 0.1% of the total radicals present, whereas ESR spectra of γ-irradiated hydrated DNA show the same radical but in much lower yields (about 0.01% at the same dose) (*4*). In this work, we continued our investigation of the effects of heavy-ion irradiation of hydrated DNA using Ar^{18+} beams. A recent report of the total yield of radicals in low-temperature, heavy-ion irradiated DNA hydrated to $\Gamma = 2.5$ (H_2O molecules/nucleotide) is in substantial qualitative agreement with the yields obtained by Becker *et al.* (*4*) using oxygen-ion beams (*5*).

We have classified the radicals observed based on their ESR dose saturation behavior and spectral breadth. The radicals $G^{+\bullet}$, $C(N3H)^{\bullet}$ and $T^{-\bullet}$ are DNA base radicals and are characterized by a small ESR spectral breadth and a clear plateau in yield at high dose. $C(N3H)^{\bullet}$ is the cytosine anion radical reversibly protonated at N3. $C(N3H)^{\bullet}$, $G^{+\bullet}$ and $T^{-\bullet}$ are designated as ''base ion radicals.'' The C1′, C3′, C4′, C5′ and $C3'_{dephos}$ radicals all have spin density largely on a single carbon and possess multiple hydrogen hyperfine couplings; these factors typically lead to ESR spectra of greater breadth than those of the base ion radicals. The C1′, C3′, C4′, C5′ and $C3'_{dephos}$ radicals are all designated as ''neutral sugar radicals.'' $TH^{\bullet}$ and $UCH_2^{\bullet}$ are designated as ''neutral base radicals.''

MATERIALS AND METHODS

Sample Preparation

Salmon testes DNA purchased from Sigma Chemical Company was used without further purification. Samples (about 150 mg as received from Sigma) were hydrated in closed systems over saturated H_2O or D_2O solutions of NaCl or KCl (*6*). Samples were then pressed into cylinders

[1] Address for correspondence: Department of Chemistry, Oakland University, Rochester, MI 48309-4477; e-mail: sevilla@oakland.edu.

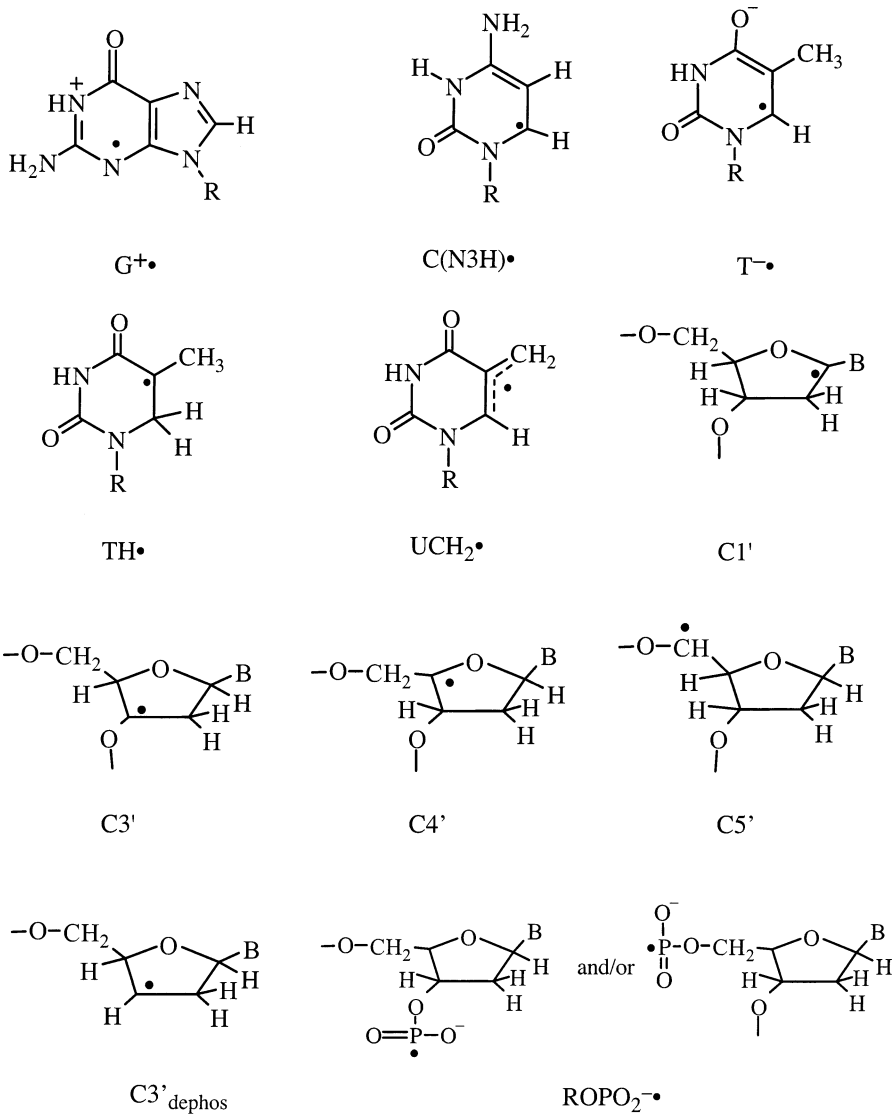

Radicals Considered in this Work

(0.4 cm diameter × ~1 cm height) or rectangular parallelepipeds (0.3 cm × 0.4 cm × ~1 cm) under a N_2 atmosphere using an aluminum die and press and were immediately frozen in liquid N_2. The actual hydration level in samples were determined by weighing the samples immediately after warming to room temperature and then again after pumping on a vacuum line overnight or after desiccation over Drierite (anhydrous $CaSO_4$) for 24–48 h; both methods of drying gave the same results. Dried samples are assumed to have a residual 2.5 water molecules per nucleotide ($\Gamma = 2.5$) which are not removed by our drying procedure (*7*). The hydration levels we report are averages over the whole sample and have relative uncertainties of ±1 D_2O/nucleotide.

Heavy-Ion Irradiation

Samples were irradiated at 77 K at the National Superconducting Cyclotron Laboratory at Michigan State University. Argon-36 and ^{40}Ar beams with specific energies of 60, 75, 80 and 100 MeV/nucleon were used; for the end points we investigated, all the beams gave similar results (within experimental error). The beam passed through approximately 5 cm of air and 1 cm of Styrofoam before encountering the sample. As an example, a 100 MeV/nucleon ^{40}Ar, beam retained a total energy of 3.88 GeV at the sample and resulted in a range of 6.80 mm in DNA hydrated to $\Gamma = 15$; for an ^{36}Ar beam (75 MeV/nucleon) with energy 2.49 GeV at the sample, the range was 3.64 mm. Since the samples used had a maximum depth of 4.5 mm, the first sample would not contain the Bragg peak and the second would. In this work, four samples contained the Bragg peak and three did not. The color development and radical formation in a single sample of 1 cm length was consistent, to within ±1 mm, with the ranges given by the TRIM program (Transport of Ions in Matter, Ziegler, IBM).

The LET in a sample was determined by using the TRIM program to estimate the energy deposited in the sample and dividing this energy by the path length of the beam in the sample. With the sample configurations used, typical LETs obtained were between 350 keV/μm and 800 keV/μm. The LET (*dE/dx*) in a single sample can vary from about 300 keV/μm at the beginning of the track to about 3800 keV/μm in the Bragg peak. For different samples in the same sample set, the average LETs, as calculated, may vary by ±25 keV/μm. All LETs reported here are rounded to the nearest ±50 keV/μm.

Ion-Beam Dosimetry

The ion-beam dosimetry is approximate. The dose in grays delivered per second in a sample (*E*) is given by

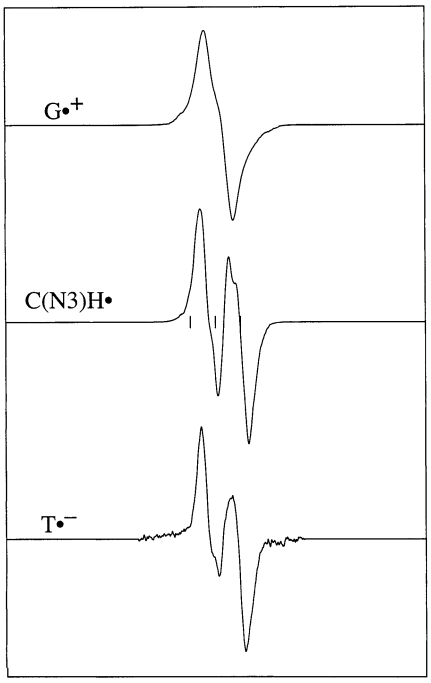

FIG. 1. Benchmark base ion-radical ESR spectra used (with $\mathcal{N}^{\cdot}$ in Fig. 2) to analyze observed DNA spectra. The origins of the spectra for $G^{+\cdot}$, $C(N3H)^{\cdot}$ and $T^{-\cdot}$ are described in Wang *et al.* (*8*). In all figures, the three vertical lines correspond to the Fremy's salt resonances with $g = 2.0056$ and $A_N = 1.309$ mT.

$$E = \frac{AN_0 f(I/I_0)I_0(10^9)(1.609 \times 10^{-19})}{FZm},$$

where A is the beam current in electrical amps, N_0 is Avogadro's constant, f is the fraction of the beam area intercepted by the sample, I_0 is the energy of the beam in gigaelectron volts, I/I_0 is the fraction of the energy of the beam deposited in the sample, F is the Faraday constant, m is the mass of the sample in kilograms, and Z is the charge on the ion for which A is determined (+18 in these experiments). The beam area was measured from the color development in a glass cover slip placed in the beam. Before any irradiations were performed, the beam current at the sample was determined by measuring, simultaneously, the current at the sample position with a Faraday cup and the upstream current. During the sample irradiation procedure, the upstream current was checked periodically; with the assumption that the ratio of sample to upstream currents is constant, the current at the sample can be calculated. The TRIM program and sample geometry were used to determine I, the energy per ion deposited in the sample; I_0 and Z were determined directly by the cyclotron settings. Typical values for these parameters, for a 0.2316-g cylindrical sample, are: $A = 15$ nA, $f = 0.47$, $I/I_0 = 0.34$, $I_0 = 3.37$ GeV, $Z = +18$. These numbers result in a dose rate of 2.0×10^3 Gy/s.

For cylindrical samples, the sample was positioned so that the ion-beam path was perpendicular to the long axis of the sample. The dose was obtained by calculating the energy (J) deposited in each of 20 slices of the cylinder (slices whose planes were parallel to the cylinder axis and ion-beam path) and dividing the sum of these energies by the total mass (kg) of the sample.

γ Irradiations

A U.S. Nuclear γ irradiator with dose rate of ~2 kGy/h was employed for all γ irradiations. Samples were irradiated under liquid nitrogen.

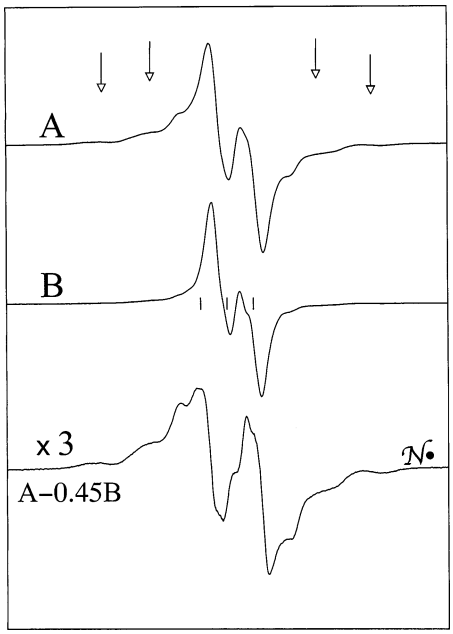

FIG. 2. Origin of benchmark composite $\mathcal{N}^{\cdot}$ spectrum. A: ESR spectrum of hydrated DNA sample (D_2O, $\Gamma = 14$) irradiated with 370 kGy (^{36}Ar, 100 MeV/nucleon, LET = 400 keV/μm). B: ESR spectrum of sample prepared and handled identically to that in A, except the dose is 35 kGy. The last spectrum, $\mathcal{N}^{\cdot}$, is obtained by computer subtraction of 0.45 B from A as described in the Materials and Methods.

Electron Spin Resonance

Spectra were generally recorded at 77 K at 45 dB (6.3 μW); for phosphorus radicals, power levels near 20 dB (2 mW) were typically used. ESR spectra were digitized and stored in a 1000-point array with field and g-value markers. A Varian Century ESR spectrometer operating at 9.2 GHz with an E-4531 dual-cavity, 9-in. magnet and low-temperature accessory was employed. Fremy's salt, with $A_N = 1.309$ mT and $g = 2.0056$, was used for field calibration and hyperfine splitting measurements; the three calibration marks shown on the spectra are the three Fremy's salt hyperfine resonances. Spectral analysis was done using programs developed in our laboratory (ESRADSUB, ESRPLAY). Spectral simulations were done with SimFonia and WINEPR (Bruker).

Computer Analysis of DNA Spectra

The low-temperature ESR spectra of irradiated, hydrated DNA samples result from the overlap of the spectra from a number of free radicals; computer deconvolution of the composite ESR spectra that result is required for the correct determination of G values (*vide infra*). Three of the four benchmark ESR spectra used for deconvolution are shown in Fig. 1. These base ion radical spectra [$G^{+\cdot}$, $C(N3H)^{\cdot}$, $T^{-\cdot}$] were obtained from experimental spectra, as described earlier (*8*). While the base ion radicals have a relatively small spectral breadth, the fourth benchmark spectrum ($\mathcal{N}^{\cdot}$), shown in Fig. 2, does not. It arises largely from a mixture of neutral radicals of generally larger hyperfine couplings and larger spectral breadth. In ion-beam-irradiated DNA, a substantial number of the radicals responsible for $\mathcal{N}^{\cdot}$ are likely to be carbon-centered radicals on the sugar moiety, such as the C1′, C3′, C4′ and C5′ (*4*) and a radical which is newly proposed in this work, a C3′-dephosphorylation radical ($C3'_{dephos}$).

$\mathcal{N}^{\cdot}$ is generated by computer subtraction of the spectrum of a 35-kGy-irradiated sample (Fig. 2B) from that of a 370-kGy-irradiated sample (Fig. 2A) to obtain a difference spectrum judged visually to be relatively free of ion-radical components. The optimum subtraction required that 45% of the intensity of the lower-dose spectrum be subtracted from 100% of

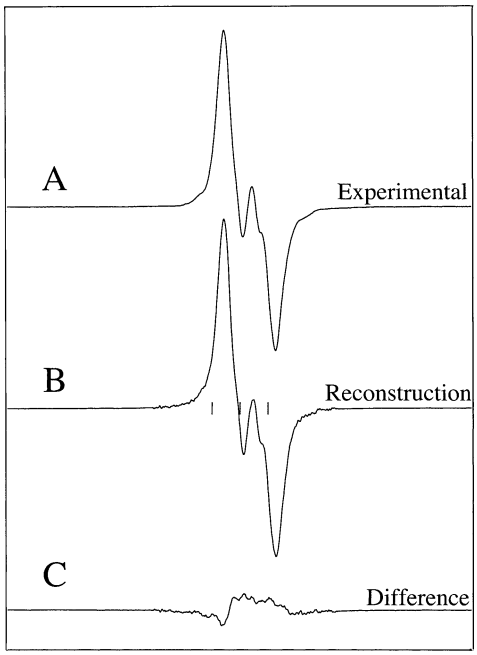

FIG. 3. A: Experimental ESR spectrum of DNA, at 77 K, hydrated to $\Gamma = 12$, irradiated with 150 kGy using an ^{40}Ar beam with energy 60 MeV/nucleon. The LET of the radiation was 800 keV/μm. B: Simulated spectrum of that shown in A, constructed using 25% $G^{+\bullet}$, 19% $C(N3H)^{\bullet}$, 18% $T^{-\bullet}$, and 38% $\mathcal{N}^{\bullet}$. C. Difference between the two previous spectra, B − A.

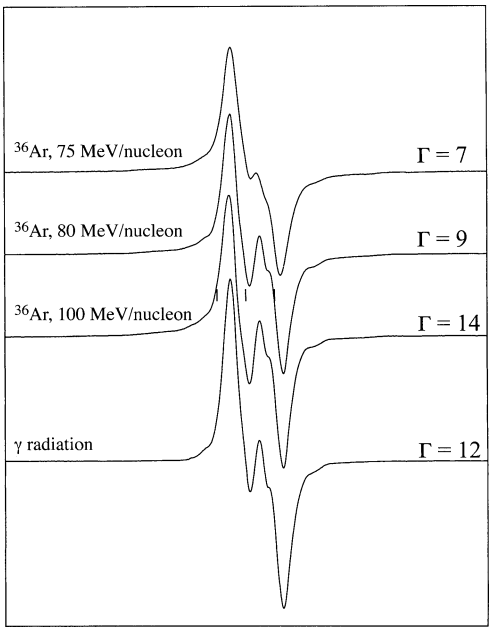

FIG. 4. ESR spectra of argon-ion-irradiated and γ-irradiated, hydrated DNA at 77 K. Beam descriptions and hydration levels are shown in the figure. The LET and dose for each beam/sample combination are: $\Gamma = 7$, 600 keV/μm, 56 kGy; $\Gamma = 9$, 650 keV/μm, 57 kGy; $\Gamma = 14$, 400 keV/μm, 33 kGy; γ radiation, 0.23 keV/μm, 40 kGy.

the higher-dose spectrum. Because the fraction of each ion radical in a composite spectra varies as a function of dose, $\mathcal{N}^{\bullet}$ may be slightly contaminated with the differences in ion-radical spectra in the central region. However, most of the signal intensity of the $\mathcal{N}^{\bullet}$ lies in the wings, which are unencumbered by this difficulty. Furthermore, the $\mathcal{N}^{\bullet}$ spectra from other subtractions at lower doses show the same spectral shape as those at higher doses, indicating that the relative contributions of the various wing components in $\mathcal{N}^{\bullet}$ remain approximately constant throughout the dose range. In addition, $\mathcal{N}^{\bullet}$ gives a linear dose response to the highest dose used, whereas the ion radicals dose-saturate readily. For this reason the separation of signals is made facile.

A least-squares fitting technique was used to find the best fit of the sum of the four benchmark spectra [$G^{+\bullet}$, $C(N3H)^{\bullet}$, $T^{-\bullet}$, $\mathcal{N}^{\bullet}$] to each experimental spectrum. A detailed description of this procedure is given in ref. (*8*) and references therein. The error measure (*err*) used to indicate the goodness of fit was calculated as shown below, in which Y is the spectral intensity and the summation is evaluated over the 1000-point array used to store the experimental and simulated spectra.

$$err^2 = \frac{\sum (Y_{simulated} - Y_{experimental})^2}{\sum (Y_{experimental})^2}$$

Typical experimental and simulated (reconstructed) spectra are shown in Fig. 3. Spectrum A shows the experimental spectrum obtained with a DNA sample at $\Gamma = 12$ and irradiated with 150 kGy ^{40}Ar. Spectrum B shows the simulated spectrum constructed using the deconvolution data obtained. In this particular case, the reconstructed spectrum contains 25% $G^{+\bullet}$, 19% $C(N3H)^{\bullet}$, 18% $T^{-\bullet}$, and 38% $\mathcal{N}^{\bullet}$. Spectrum C is the difference of the two spectra, B − A and, for this analysis, $err = 0.11$. For the reconstructions used in this work, err^2 varied from 0.0016 to 0.012, giving *err* values from 0.04 to 0.11. The radical fractions obtained are reproducible to within a few percent, but the absolute accuracy is likely to be substantially less (~10%) and may change as our understanding of these systems improves. It should be noted that computer analysis of overlapped ESR spectra was performed with D_2O-hydrated DNA because the improved resolution (relative to H_2O hydration) allows for more accuracy in the results of the deconvolution.

Calculation of G and k Values

Using the deconvolution results, it was possible to obtain dose–response relationships for each of the radicals/benchmark spectra used, that is, the individual base ion radicals and $\mathcal{N}^{\bullet}$. For each of the three base ion radicals, the dose response followed relationship (1) (*7*, *9*, *10*), in which Y is the yield of radicals in μmol/kg, G is the low-dose yield in μmol/J, k is the destruction constant in Gy^{-1}, and D is the dose in Gy. G/k equals the plateau yield, Y_∞, in μmol/kg.

$$Y = (G/k)(1 - e^{-kD}). \quad (1)$$

In this work, unless otherwise stated, the G reported for an overall mixture of radicals is the sum of the individual G values obtained by computer deconvolution of ESR spectra followed by individual determination of each radical G value. This was necessary because the destruction constants for the various radicals differ considerably; specifically, the destruction constant for $\mathcal{N}^{\bullet}$ is much smaller than that of the ion radicals.

RESULTS

Figure 4 shows the ESR spectra of DNA, at various hydrations, irradiated with argon beams or with γ radiation. The LETs for the beams used are shown in Table 1. The overall appearance of the spectra for the argon-ion-irradiated samples is similar to that obtained from γ-irradiated samples at similar hydration and dose (*7*, *8*); however, there is a noteworthy difference between the different irradiations. The argon-ion-irradiated samples show spectral components in the wings of the spectra that are present in much higher relative intensities than in γ-irradiated samples at the same dose. The wing components increase in intensity as

TABLE 1
***G* and *k* Values for Argon-Ion-Irradiated DNA**

Beam	LET[a] (keV/μm)	Γ (H_2O/ nucleotide)	$G(G^+)$[b] k[c]	$G(C(N3H))$[b] k[c]	$G(T^-)$[b] k[c]	$G(A^-)$[b] k[c]	$G(\mathcal{N}^\cdot)$[b]	G(total)[b]
^{36}Ar, 75 MeV/nucleon	600	7	0.010	0.007	0.011	0.011	0.010	0.049
			0.49	1.8	0.58	0.82	—	
^{36}Ar, 80 MeV/nucleon	650	9	0.037	0.020	0.028	0	0.021	0.106
			1.4	0.55	1.9	—	—	
^{40}Ar, 100 MeV/nucleon	350	12	0.046	0.036	0.034	0	0.032	0.148
			2.8	1.9	3.3	—	—	
^{36}Ar, 75 MeV/nucleon	600	12	0.043	0.032	0.029	0	0.032	0.136
			1.1	0.68	1.6	—	—	
^{40}Ar, 60 MeV/nucleon	800	12	0.018	0.014	0.013	0	0.018	0.063
			0.73	0.69	0.94	—	—	
^{36}Ar, 100 MeV/nucleon	400	14	0.030	0.033	0.039	0	0.037	0.139
			1.1	1.2	2.5	—	—	
^{40}Ar, 80 MeV/nucleon	500	16	0.064	0.050	0.035	0	0.062	0.211
			1.6	0.88	1.6	—	—	

[a] $\pm$50 keV/μm.
[b] μmol/J; estimated error in G is $\pm$35%.
[c] $\times 10^5$, Gy^{-1}; estimated error in k is $\pm$50%.

dose is increased and are also clearly visible in the high-dose spectrum shown in Fig. 2A (arrows). As in our earlier work with oxygen-ion beams (see Discussion) (*4*), we attribute these wing components, which are also clearly associated with the benchmark spectrum $\mathcal{N}^\cdot$ (Fig. 2), to neutral, carbon-centered radicals located primarily on the deoxyribose sugars. In Fig. 5, we show the dose–response curves for all the samples presented in this work. Each point plotted in this figure represents a single sample; for example, for the data shown for a hydration of $\Gamma = 7$, the three points shown result from three different samples prepared and handled in an identical fashion, but irradiated with different doses. Two *approximate* trends are evident in this figure. As the hydration level increases, the concentration of radicals stabilized at 77 K increases. Also, higher LETs lead to a lower concentration of stabilized radicals at 77 K. The lines drawn in Fig. 5 show the total radical yields with dose. *G* and *k* values were determined using individual radical yields (see Materials and Methods). A significant feature of the argon-ion dose–yield curves in Fig. 5 is that the curves show no plateaus; in contrast, a clear plateau is found in the dose–yield curves for γ-irradiated DNA samples (*7, 8*). As can be seen, the yields at high doses for argon-ion-irradiated samples far exceed those for the γ-irradiated sample even though the *G* values for ion radicals are lower for argon-ion-irradiated samples. This is explained by the substantially larger *G* value for neutral radicals in argon-ion-irradiated samples relative to γ-irradiated samples, combined with low destruction constants for neutral radicals for both radiations. The increased formation of radiation insensitive neutral radicals in DNA samples irradiated with argon ions is then a fundamental characteristic of the heavy-ion beams.

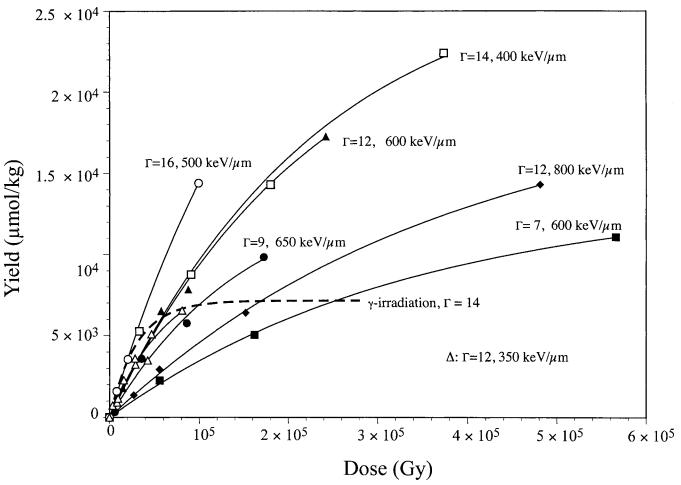

FIG. 5. Dose responses of all samples presented in this work. Each individual curve was generated by irradiating a series of identically prepared samples with different doses (see the Materials and Methods). A general, but not inviolate, trend of increasing yields with increasing hydration and decreasing LET is evident. Lines are drawn for the eye only. The experimental curve (dashed) for γ-irradiated DNA ($\Gamma = 14$), is from ref. (*7*) and is shown for comparison purposes. It shows a higher initial yield but a lower yield at high doses, owing to the production of fewer neutral radicals.

Figure 6 is an example of the dose response obtained for each of the benchmark base ion radicals [$G^{+\cdot}$, $C(N3H)^\cdot$, $T^{-\cdot}$] and for the composite spectrum $\mathcal{N}^\cdot$, obtained after computer analysis of a composite ESR spectrum. The data shown are for a set of samples at $\Gamma = 14$, irradiated with a 100 MeV/nucleon ^{36}Ar beam, resulting in an LET of 400 keV/μm (open squares in Fig. 5). The overall appearance of the response is quite typical of that found in argon-ion-irradiated samples. The base ion radical yields reach a plateau; their behavior can be fitted using Eq. (1), which gives the *G* values reported in Table 1. As can be seen, however, the composite spectrum $\mathcal{N}^\cdot$ yield displays a linear dose response up to the highest dose used; other samples behaved

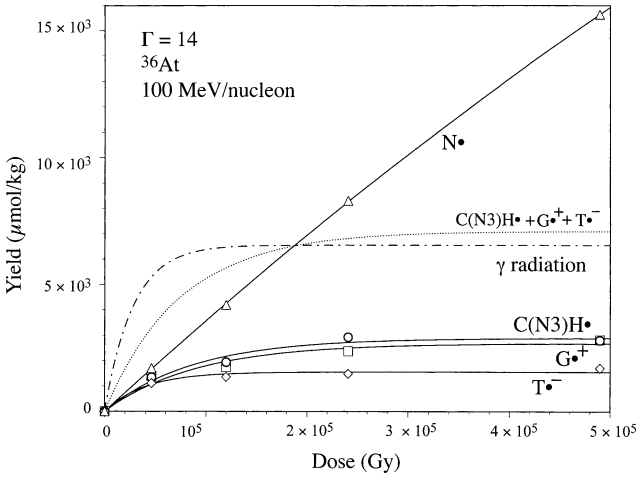

FIG. 6. Results of analysis, for individual radicals, of a hydrated DNA sample set, at 77 K, hydrated to $\Gamma = 14$, and irradiated with an ^{36}Ar beam, resulting in an LET of 400 keV/μm (open squares in Fig. 5), using benchmark spectra shown in Fig. 1 and $\mathcal{N}^{\cdot}$ from Fig. 2. The base ion radicals reach a plateau in yield; the lines for each are the fit to Eq. (1). The mix of radicals represented by $\mathcal{N}^{\cdot}$ does not reach a plateau and is fitted to a straight line. The *G* value and *k* value obtained for each base ion radical and the *G* value obtained for $\mathcal{N}^{\cdot}$, from the line fits shown, are given in Table 1. The curve for γ-irradiated DNA is calculated (using Eq. 1) from *G* and *k* values for all ion radicals for a DNA sample hydrated to $\Gamma = 14$ (ref. *7*).

similarly. For $\mathcal{N}^{\cdot}$, the *G* values obtained as the slopes of the observed dose–response lines are also given in Table 1. Table 1 also includes the destruction values, *k*, obtained for each base ion radical obtained from the fit of the dose–response data to Eq. (1). The *k* values obtained from argon-ion-irradiated DNA generally follow the trend observed with γ-irradiated DNA; C(N3H)$^{\cdot}$ has the smallest *k*, $G^{+\cdot}$ the next largest, and $T^{-\cdot}$ the largest. However, the *k* values observed with argon-ion irradiation are typically smaller than those observed with γ irradiation. This is likely due at least in part to the partition of energy between the high-energy-density region and the γ-radiation-like region of the track. Using Eq. (1) and typical measured *G* values for $\mathcal{N}^{\cdot}$, the maximum possible value of *k* for $\mathcal{N}^{\cdot}$ was estimated to be 4×10^{-6} Gy^{-1}; larger values result in noticeable curvature in the dose–response curve calculated from Eq. (1), a curvature not present in the observed data (Fig. 6).

The behavior of the base ion-radical dose responses with argon-ion irradiation is qualitatively similar to that observed with γ-irradiated DNA (*8*). The yield of these radicals reaches a plateau at relatively low doses; in addition, the plateau yields of base radicals for argon-ion-irradiated samples and for γ-irradiated samples, at the same hydration levels, are the same, within experimental error (estimated to be ±30%). In Fig. 6 we compare the yield of base ion free radicals for γ- and argon-ion-irradiated DNA at the same hydration level ($\Gamma = 14$). These results indicate that the DNA base ion radical saturation yield appears to be independent of the LET of the radiation; this would be expected if the ion radical production and destruction were largely from the low-LET component of the high-LET beam, i.e., the δ rays, which extend from the track core.

TABLE 2
Comparison of Argon-Ion and γ-Irradiated Samples

Γ (H_2O/ nucleotide)	LET (keV/μm)	*G*(overall, argon)[a]	*G*(overall, γ)[a,b]	Fraction ($\mathcal{N}^{\cdot}$, argon)[c]
7	600	0.049	0.156	0.20
9	650	0.106	0.172	0.20
12	350	0.148	0.207	0.22
12	600	0.136	0.207	0.24
12	800	0.063	0.207	0.29
14	400	0.139	0.234	0.27
16	500	0.211	0.267	0.29

[a] μmol/J; estimated error in *G* is ±35%.
[b] Ref. (*7*).
[c] $G(\mathcal{N}^{\cdot}, \text{Ar})/G(\text{overall, argon})$.

In addition, at the same hydration level, the composition of the ion radical cohort is similar in γ-irradiated samples and argon-ion-irradiated samples. For example, at $\Gamma = 9$ (^{36}Ar, 80 MeV/nucleon), the fractional amount of each ion radical found (in the whole ion radical cohort, not including neutral radicals) at low dose, as determined by *G* values, is $G^{+\cdot}$, 0.44; C(N3H)$^{\cdot}$, 0.24; and $T^{-\cdot}$, 0.33. For γ-irradiated samples at the same hydration, the fractional amounts are: $G^{+\cdot}$, 0.42; C(N3H)$^{\cdot}$, 0.28; and $T^{-\cdot}$, 0.30 (*8*). These values are reproducible to within 0.05 fractional units. Thus the three ion radicals are formed in about the same relative amounts by γ and argon-ion irradiation. A similar correspondence between γ and argon-ion irradiation was found for each of the sample sets investigated at the various hydration levels used, within the ±30% estimated experimental error.

The Neutral Radicals

Whereas the ion radical plateau yields for argon-ion- and γ-irradiated DNA are the same within experimental error, the yields of neutral radicals are significantly higher for argon-ion-irradiated samples than for similar γ-irradiated samples. This is illustrated by the curves for DNA hydrated to $\Gamma = 14$ shown in Fig. 6. The curve shown for γ-irradiated DNA (*7*) shows far lower total yield at high doses because ion radicals dominate the γ-irradiated DNA spectrum; on the other hand, neutral radicals ($\mathcal{N}^{\cdot}$), which are less susceptible to radiation destruction, dominate the spectrum of argon-ion-irradiated DNA at high doses. In argon-ion-irradiated samples, the fraction of neutral radicals found (using fraction $= G_{\mathcal{N}^{\cdot}}/G_{\text{total}}$) increases from 0.20 at $\Gamma = 7$ to 0.29 at $\Gamma = 16$ in the LET range 350–650 keV/μm (Table 2); one data set with LET = 800 keV/μm at $\Gamma = 12$ gave a fraction of 0.29. In typical γ-irradiated samples, neutral radicals (as designated by a composite spectrum similar to $\mathcal{N}^{\cdot}$) make up about 0.07 of the initial yield of radicals in low-dose samples hydrated to $\Gamma = 16$ (*4*).

In Fig. 7 we show the benchmark spectrum used for $\mathcal{N}^{\cdot}$

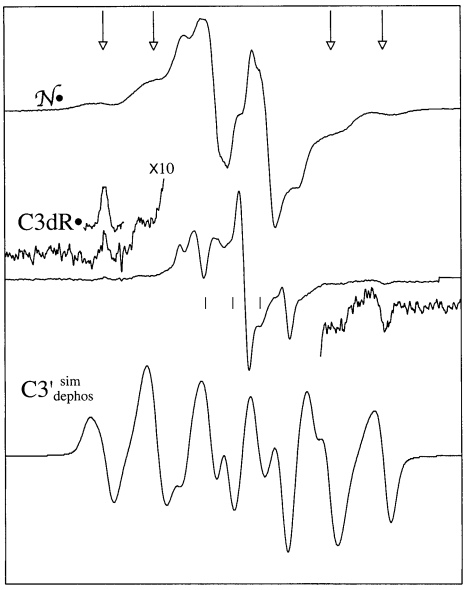

FIG. 7. $\mathcal{N}^{\cdot}$ is the benchmark ESR spectrum as shown in Fig. 2. C3dR• is the ESR spectrum of 2′, 3′-dideoxy-3-acetylribose in 8 *M* $NaClO_4$ glass, obtained at 77 K after photolysis for 45 min with a Hg-Xe UV lamp filtered at 320 nm and warming to eliminate $O^{-\cdot}$. The outer two line components in each wing (arrows) are attributed to C3dR•. The inner part of the spectrum arises from both the inner lines of C3dR•, as well as from other radicals formed by the photolysis (and by $O^{-\cdot}$ attack on 2′, 3′-dideoxy-3-acetylribose). The expanded spectrum is obtained by digitally multiplying the original spectrum by 10; the downfield single peak expansion was obtained after further warming. The bottom spectrum is a computer-simulated ESR spectrum of $C3'_{dephos}$ using parameters given in the Results. The outer two line components in each wing correspond to those visible in $\mathcal{N}^{\cdot}$ and in the C3dR• spectrum.

(as in Fig. 2). The $\mathcal{N}^{\cdot}$ spectrum contains line components that coincide with those found in the C1′ spectrum (*4, 11–14*), those expected in the C3′ and/or C4′ spectrum (which may be very similar to each other) (*4, 11, 14, 15*), and a doublet that is associated with the C5′ radical (*11, 16*); this suggests that the $\mathcal{N}^{\cdot}$ spectrum arises, in large part, from radicals which are stabilized on the sugar moiety. The $\mathcal{N}^{\cdot}$ spectrum was also compared with a variety of spectra from neutral radicals known to form on the DNA bases; for the most part, these did not match the $\mathcal{N}^{\cdot}$ spectrum as well as the sugar moiety radicals. In addition, $\mathcal{N}^{\cdot}$ does not show the outer line components of the TH•/TD• spectrum (*14, 17*) in any significant amounts. The thymine allyl radical ($UCH_2^{\cdot}$) (*14, 18*) displays some line components similar to the C1′ radical spectrum; it may also be present in small amounts in the $\mathcal{N}^{\cdot}$ spectrum. In summary, $\mathcal{N}^{\cdot}$ appears to contain substantial contributions from deoxyribose radicals including a newly proposed deoxyribose radical ($C3'_{dephos}$).

A Proposed New Sugar Radical in Irradiated DNA

The outer line components of $\mathcal{N}^{\cdot}$, 134 G in breadth (Fig. 7, outer arrows), do not correspond to any previously characterized DNA sugar or base radical (*3, 14, 16, 19, 20*). The considerable breadth of the ESR spectrum suggests a radical with spin density localized on a single carbon atom and hyperfine interactions with at least four hydrogen atoms; a radical formed by dephosphorylation at the C3′ carbon of the deoxyribose ($C3'_{dephos}$) is a reasonable candidate for such a radical.

A variety of experimental and theoretical tests were performed to test our assignment of the outer spectral line components to $C3'_{dephos}$. First, we performed a density functional theory calculation on the model radical $C3'_{model}$(I) which was optimized at the B3LYP 6-31G+(D) level (Gaussian 98) from a B-DNA starting conformation that was minimized by molecular mechanics. Optimizations from other starting geometries (PM3 optimized structure, forced planar structure) gave the same result, suggesting a global minimum had been obtained. Hyperfine couplings calculated at this level were 26.9 G (H2a), 49.1 G (H2b), −23.4 G (H3), and 34.9 G (H4); the sum of the magnitudes of these is 134 G. We have also performed calculations on the C3′• of a dCMP analogue by replacing the NH_2 group in the previously optimized model compound with cytosine and the 5′-OH with a methyl phosphate anion. This structure, $C3'_{model}$(II), was allowed to undergo 10 additional optimization iterations (not fully minimized). The resultant conformation and hyperfine couplings [27.7 G (H2a), 48.0 G (H2b), −23.5 G (H3), 37.8 G (H4), sum = 137 G] were similar to those found for the smaller model system, which shows that the influence of the DNA base and phosphate group on the couplings is modest. On the other hand, the β-couplings should be very sensitive to the deoxyribose conformation, and it would be expected that the local environment would perturb the structure about the global minimum and thus alter β-proton couplings somewhat. This suggests that in DNA a variety of conformations could substantially broaden the line components of the $C3'_{dephos}$ radical.

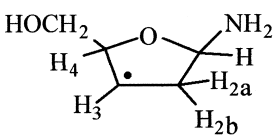

C3'model(I)

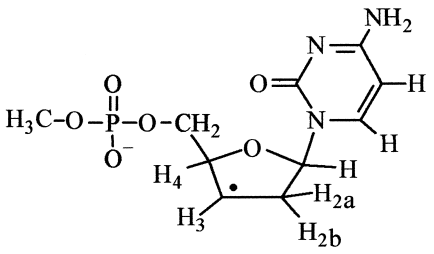

C3'model(II)

An ESR spectrum simulation carried out to second order, without forbidden transitions, for $C3'_{dephos}$ using a single anisotropic hydrogen atom with a hyperfine coupling [Ax, Ay, Az] of [−11 G, −23.4 G, −34 G] and three hydrogen atoms with isotropic couplings of 26.9 G (1H), 34.9 G (1H) and 49.1 G (1H), with $g_x = 2.0036$, $g_y = 2.0023$ and $g_z = 2.0044$ and linewidth = 6 G results in the spectrum shown in Fig. 7 ($C3'^{sim}_{dephos}$). As can be seen, the four outer line components of the simulation are a close match to those visible in the spectrum of $\mathcal{N}^{\cdot}$.

An experimental confirmation of the expected ESR spectrum was obtained by synthesis of a model of the $C3'_{dephos}$ radical. UV photolysis of 2,3-dideoxy-3-acetylribose (synthesis to be published) at 320 nm, in 8 *M* $NaClO_4$ results in α-cleavage of the acetyl group-sugar bond (*21*) and a radical (C3dR•) similar in structure to the proposed $C3'_{dephos}$ radical. We note that this reaction has a low yield in solid matrices, owing to cage effects which encourage substantial recombination.

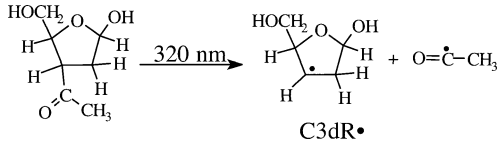

C3dR•

The spectrum of the radical obtained (C3dR•) is shown in Fig. 7. The outer spectral components of C3dR• are separated by ∼134 G, as are those found in the spectrum of $\mathcal{N}^{\cdot}$; the next inner components of $\mathcal{N}^{\cdot}$, separated by ∼83 G, are also clearly visible in the spectrum of C3dR• (Fig. 7). The line shapes for the C3dR• do differ from that found for $\mathcal{N}^{\cdot}$, perhaps owing to the many different local environments found in the DNA system. Furthermore, the sample was annealed to remove the signal from $O^{-\cdot}$, resulting in a large background signal from the $^{\cdot}CH_2C(O)$-R. Overall, these results lend support to our assignment of the outer spectral components in $\mathcal{N}^{\cdot}$ to the $C3'_{dephos}$ radical.

Figure 8A shows the experimental ESR spectrum of a DNA sample, hydrated to Γ = 9, irradiated with 170 kGy with an 80 MeV/nucleon ^{36}Ar beam. The spectrum is taken over a wide field sweep (1600 G) to show the components of a phosphorus-centered radical. This spectrum is, within experimental limits, identical to that obtained with ^{18}O-ion-irradiated DNA (*4*) and assigned to an $ROPO_2^{-\cdot}$. Panel B shows a simulated ESR spectrum, including second-order effects, using phosphorus atom couplings of $A_{xx} = A_{\|} = 775$ G, $A_{yy} = A_{zz} = A_{\perp} = 610$ G, $g_{xx} = g_{\|} = 2.00$, $g_{yy} = g_{zz} = g_{\perp} = 2.01$ and a gaussian line shape with linewidth 12 G. This spectrum matches the experimental spectrum well; the couplings are the same as found for ^{18}O-ion-irradiated samples (*4*). Using standard double integration techniques, we estimate that there are approximately one or two phosphoryl radicals per thousand radicals in this argon-ion-irradiated sample. Previously, in ^{18}O-ion-irradiated samples, one phosphoryl radical per thousand was found.

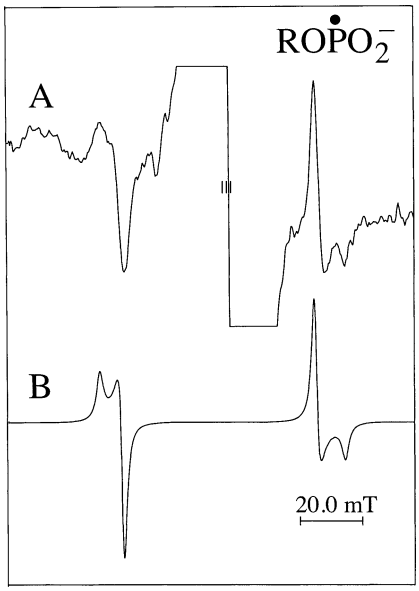

FIG. 8. ESR spectra of phosphorus centered radical. A: Spectrum of DNA hydrated to Γ = 9 and irradiated with a ^{36}Ar-ion beam, 80 MeV/nucleon (650 keV μm), with a dose of 170 kGy at 77 K. The spectrum of a phosphoryl radical, $ROPO_2^{-\cdot}$, is evident in the wings. B: Simulated spectrum of $ROPO_2^{-\cdot}$ using parameters given in the Results. The spectrum is calculated to second order because of the large phosphorus hyperfine coupling constants involved.

DISCUSSION

Yields, Destruction Constants and Track Structure

For heavy-ion-irradiated samples, relative to γ-irradiated samples, we attribute the differences in observed *G* values, *k* values and radical formation to the different track structures of the respective radiations. There are a variety of approaches to the theoretical description of heavy-ion track structure (*22–27*), but all share the feature of positing two distinct regions of energy deposition. In one region, models suggest large individual energy depositions, high energy densities, and formation of a track core; the core may be fragmented or contiguous, depending on the LET. The high-energy events in the core may involve multiple and/or proximate ionizations, nuclear displacements and Coulomb explosions. The second region is formed by high-energy electrons (δ rays) that travel away from the core and generate a region of non-overlapping, γ-radiation-like spurs. Radical formation processes in this region are similar to those found in samples exposed to low-LET radiation. Both the energy partition between the core and γ-radiation-like regions, and the different processes that occur in each are likely causes of the different results observed with γ-irradiated samples relative to heavy-ion-irradiated samples.

Hydration and G Values

As the hydration level increases, the observed yields trend upward (Table 1); a similar effect was observed in γ-irra-

diated DNA in the same hydration range (*7*). This effect likely has several origins. First, an increased amount of water surrounding the DNA results in increased shielding of primary ion radicals from each other, thereby resulting in slower recombination at all stages of radical development and stabilization; this causes an increase in radical yield as hydration increases. Second, as the number of waters of hydration increases, steric interactions cause an increase in the separation of each double helix from its neighbors; this decreases the rate of electron tunneling from electron traps to holes (*28, 29*), thereby decreasing the recombination of charged radicals. Last, hydration waters provide basic sites for the deprotonation of cation radicals to form neutral radicals; thus, as hydration increases, more carbon-centered neutral radicals are able to form and stabilize at 77 K. As expected from this effect, $G(\mathcal{N}^{\cdot})$ tends to increase with increased hydration in argon-ion-irradiated samples (Table 1).

Radiation Quality and Radical Yields

Argon-ion irradiation results in a lower overall yield (*G* value) of radicals and higher yields of neutral radicals than γ irradiation (Tables 1, 2). Other workers, using DNA and DNA components, have also observed a diminution in the overall *G* of free radicals stabilized at 77 K, relative to γ-irradiated samples, with high-LET heavy-ion irradiation (*5, 30*). In the high-energy-density track core, electrons and holes are formed very close to each other, and recombination, due to coulomb attractions, lowers the yield of trapped primary ion radicals. In addition, in the core, the normally stable (at 77 K) ion radicals [$G^{+\cdot}$ and $T^{-\cdot}$, and the reversibly protonated C(NH3)$^{\cdot}$] that do form are likely to be trapped closer to each other than in γ-irradiated samples; this permits faster electron tunneling and more destruction of these radicals than in low-LET-irradiated samples. We note that previous work suggests that all electrons and holes trapped within 3.5 nm will recombine (*7, 8*), so the number of ion radicals that are trapped in our experiments is very sensitive to the density of ionizations. As a consequence, trapped ion radicals formed and stabilized by argon-ion irradiation at 77 K originate predominantly from the low-LET region of the track. Both the similar saturation yields (Fig. 6) and the similar composition of the ion-radical cohort found in γ-irradiated samples and argon-ion-irradiated samples are consistent with this assertion.

With the assumption that ion radicals are formed predominantly in the low-LET region of the argon-ion-irradiation track, comparison of the relative *G* values of ion radicals for argon-ion- and γ-irradiated samples gives an estimate of the partition of energy between the track core and the low-LET region. For the five samples with $9 \leq \Gamma \leq 16$ and LET ≤ 650, $G_{\text{ions}}(\text{Ar})/G_{\text{ions}}(\gamma)$ is in the range 0.49 to 0.56, suggesting that roughly half of the energy in the track is deposited in the core; for the remaining two samples (one at low hydration and one at high LET), $G_{\text{ions}}(\text{Ar})/G_{\text{ions}}(\gamma)$ are near 0.25, indicating that about 75% of the energy is in the core. Thus our results suggest the energy partitioned to the core lies in the range of 50% to 75% for the conditions we have investigated.

The Neutral Radicals

Based on the foregoing arguments, we assign the majority of neutral radicals found at 77 K (and represented by the benchmark ESR spectrum $\mathcal{N}^{\cdot}$) to the track core. In considering their formation, two distinct differences between argon-ion irradiation and γ irradiation exist. First, with high-LET radiation, the high deposition of energy increases the rate and proximity of a number of processes that normally occur more slowly and are dispersed in low-LET processes; there also exist processes unique to high-LET radiation such as nuclear knock-ons and coulomb explosions (*22*).

Many of the neutral sugar radicals of concern can be formed by ionization of the deoxyribose sugar moiety [S(H)] and deprotonation of the cation radical thus formed (Scheme 1, path B); the yield of neutral radicals does increase as the level of hydration increases, both for argon-ion-irradiated (Table 2) and γ-irradiated (*8*) DNA, suggesting that sugar cation-radical deprotonation does play a part in their formation. Product analyses for DNA γ-irradiated at room temperature suggests that approximately one-third of the holes formed in the sugar moiety shown in Scheme 1 transfer to the bases (*31*); at 4 K, similar product analyses suggest that about half do so (*32*).

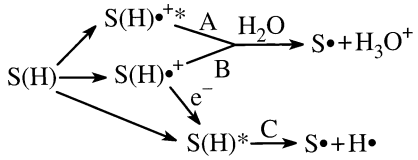

Scheme 1

It is also reasonable to expect that excited states in combination with sugar or base cation radicals would enhance deprotonation reactions (Scheme 1, path A). Combinations of excited states with cation radicals would be much more likely to occur using high-LET radiation relative to low LET and may explain in part the increased yield of neutral radicals in high-LET processes relative to lower LET. We note that deprotonation of excited-state cations has been suggested in the radiolysis of solid-state hydrocarbons (*33–36*). Excited states from recombinations of electrons and holes on the sugar moieties or direct excitations that lead to homolytic bond cleavage are other possible paths to sugar radicals (path C).

The C3′ Radical from Dephosphorylation ($C3'_{dephos}$)

Based on the known reactions of phosphodiesters, the neutral $C3'_{\text{dephos}}$ radical may result from scission of the C3′–O bond by dissociative electron attachment (Scheme 2); thus its formation is accompanied by an immediate strand break.

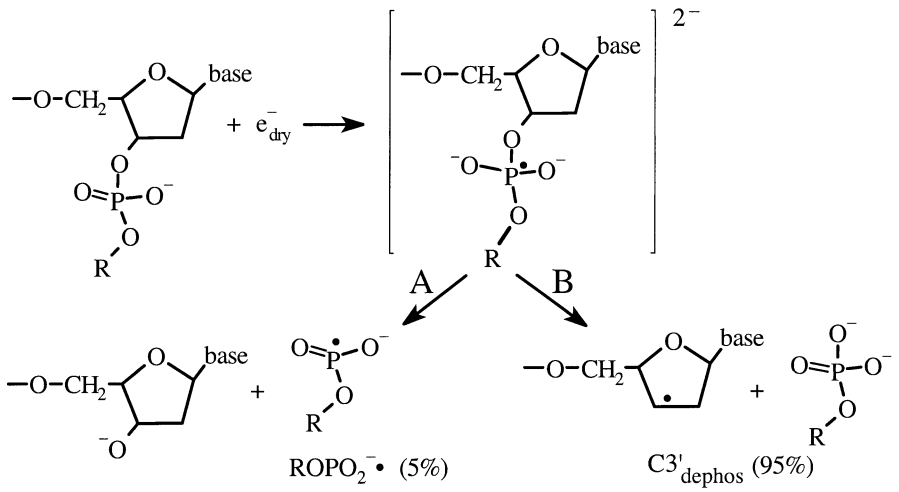

Scheme 2

This mechanism for reaction of phosphodiesters has been well characterized (*37–41*). The attack by an electron leads to one of two possible radical products depending on the path taken, as shown in Scheme 2. In earlier work, we reported formation of the phosphoryl radical (path A) in oxygen-beam-irradiated DNA and recognized that the C3′ dephosphorylation radical should also be formed (*4*). Our evidence suggests that both $C3'_{dephos}$ and $ROPO_2^{-\bullet}$ are formed in this work by high-LET radiation in accord with paths A and B. It is pertinent to note that in irradiated aqueous DNA, it is well established that hydrated electrons do not cause strand breaks (*24*, *42*, *43*). Nor do we expect electrons trapped on the DNA bases to do so (*3*). In the process pictured in Scheme 2, the electron is not solvated; rather, it is non-thermal, perhaps possessing several electron volts of energy. In fact, recent work has shown that resonant absorption of low-energy (3–10 eV) electrons results in a variety of damage to DNA, including single- and double-strand breaks (*44–46*). We believe that these processes are likely to be important in the dissociative electron attachment reactions proposed in Scheme 2.

We estimate that $C3'_{dephos}$ contributes approximately about 3 to 4% of total radicals compared to 0.1–0.2% for phosphorus-centered radicals. The more than one order of magnitude greater yield of the $C3'_{dephos}$ radical over the yield of phosphorus-centered radicals suggests that path B greatly dominates over path A (Scheme 2). We note similar results are found in irradiated alkyl phosphates (*37–41*).

Radiation Quality and k Values

The *k* values obtained offer some insight into the track structure of the argon-ion irradiation. k^{-1} is defined as D_0, the dose required to destroy 0.63, $(1 - e^{-1})$, of the previously trapped radicals in a sample. Thus it is a measure of the sensitivity of trapped free radicals to destruction by radiation; a large *k* implies a high sensitivity to radiation destruction. For γ irradiation, some irregular variations in the *k* value with hydration were found between $\Gamma = 6$ and $\Gamma = 18$. The overall differences in these values for the different radicals were considered to be due to the charge state of each respective radical; charged radicals ($T^{-\bullet}$, $G^{+\bullet}$) are more likely to undergo combination reactions with radiation-produced electrons and holes than uncharged radicals ($C(N3H)^{\bullet}$), and thus they are more susceptible to destruction by radiation.

In this current work, 22 different *k* values were determined for argon-ion-irradiated samples over a range of hydrations ($\Gamma = 7$ to 16) and LETs (350–800 keV/μm) (Table 1). Uncertainty in the data does not permit rigorous correlation to be made between the *k* values found and LET or between *k* values and Γ; however, some overall trends are quite clear. The general trend in the *k* values found for γ radiation, $k[C(N3H)^{\bullet}] < k(G^{+\bullet}) < k(T^{-\bullet})$, was also found for argon-ion irradiation (Table 1); this is to be expected if the majority of radical destruction occurs by overlap of the γ-ray-like region of one track with the γ-ray-like region of a second. In addition, for 21 of the 22 values measured, $k(\mathrm{Ar}) < k(\gamma)$, that is, $D_0(\mathrm{Ar}) > D_0(\gamma)$. Thus much of the of the energy deposited using argon-ion irradiation is ineffective, relative to γ irradiation, in destroying previously trapped radicals. Even so, the steady-state ''plateau'' yields of ion radicals are the same in the two radiations, suggesting that the maximum ion radical concentrations are determined by the nature of DNA itself. The substantial differences in the yield of neutral radicals that have very small destruction constants account for the larger overall high-dose yields found in ion-beam-irradiated samples.

ACKNOWLEDGMENTS

This research was supported by NIH NCI Grant RO1CA45424 and by the Oakland University Research Excellence Fund. The assistance of Dr. Reginald Ronningen and Dr. R. Anantaraman of the National Superconducting Cyclotron Laboratory at Michigan State University and the help

of the laboratory staff during the heavy-ion beam irradiations are gratefully acknowledged.

Received: August 21, 2002; accepted: April 23, 2003

REFERENCES

1. M. G. Debije, Y. Razskazovskiy and W. A. Bernhard, The yield of strand breaks resulting from direct-type effects in crystalline DNA x-irradiated at 4 K and room temperature. *J. Am. Chem. Soc.* **123**, 2917–2918 (2001).
2. M. G. Debije and W. A. Bernhard, Thermally stable sites for electron capture in directly ionized DNA: Free radicals produced by the net gain of hydrogen at C5/C6 of cytosine and thymine in crystalline oligodeoxynucleotides. *J. Phys. Chem. A* **106**, 4608–4615 (2002).
3. D. Becker and M. D. Sevilla, The chemical consequences of radiation damage in DNA. *Adv. Radiat. Biol.* **17**, 121–180 (1993).
4. D. Becker, Y. Razskazovskii, M. U. Callaghan and M. D. Sevilla, Electron spin resonance of DNA irradiated with a heavy-ion beam ($^{16}O^{8+}$): Evidence for damage to the deoxyribose phosphate backbone. *Radiat. Res.* **146**, 361–368 (1996).
5. B. Weiland and J. Hüttermann, Free radicals from lyophilized 'dry' DNA bombarded with heavy-ions as studied by electron spin resonance spectroscopy. *Int. J. Radiat. Biol.* **75**, 1169–1175 (1999).
6. S. G. Swarts, M. D. Sevilla, D. Becker, C. J. Tokar and K. T. Wheeler, Radiation-induced DNA damage as a function of hydration. I. Release of unaltered bases. *Radiat. Res.* **129**, 333–344 (1992).
7. W. Wang, D. Becker and M. D. Sevilla, The influence of hydration on the absolute yields of primary ionic free radicals in γ-irradiated DNA at 77 K. I. Total radical yields. *Radiat. Res.* **135**, 146–154 (1993).
8. W. Wang, M. Yan, D. Becker and M. D. Sevilla, The influence of hydration on the absolute yields of primary ionic free radicals in gamma irradiated DNA at 77 K. II. Individual radical yields. *Radiat. Res.* **137**, 2–10 (1994).
9. J. P. Elliot and S. J. Wyard, Radical yields. In *Effects of Ionizing Radiation on DNA* (J. Hüttermann, W. Köhnlein and R. Teoule, Eds.), pp. 80–96. Springer-Verlag, New York, 1978.
10. R. A. Spalletta and W. A. Bernhard, Free radical yields in A:T polydeoxynucleotides, oligodeoxynucleotides and monodeoxynucleotides at 4 K. *Radiat. Res.* **130**, 7–14 (1992).
11. M. E. Malone, P. M. Cullis, M. C. R. Symons and A. W. Parker, Biphotonic photo-ionization of cytosine and its derivatives with uv radiation at 248 nm: An EPR study in low temperature perchlorate glasses. *J. Phys. Chem.* **99**, 9299–9308 (1995).
12. Y. Razskazovzkii, M. Roginskaya and M. D. Sevilla, Modification of the reductive pathway in gamma-irradiated DNA by electron scavengers: Targeting the sugar-phosphate backbone. *Radiat. Res.* **149**, 422–432 (1998).
13. W. Wang and M. D. Sevilla, Reaction of cysteamine with individual DNA base radicals in γ-irradiated nucleotides at low temperature. *Int. J. Radiat. Biol.* **66**, 683–695 (1994).
14. B. Weiland and J. Hüttermann, Free radicals from X-irradiated 'dry' and hydrated lyophilized DNA as studied by electron spin resonance spectroscopy: analysis of spectral components between 77 K and room temperature. *Int. J. Radiat. Biol.* **74**, 341–358 (1998).
15. M. G. Debije and W. A. Bernhard, Electron paramagnetic resonance evidence for a C3′ sugar radical in crystalline d(CTCTCGAGAG) X-irradiated at 4 K. *Radiat. Res.* **155**, 687–692 (2002).
16. D. M. Close, Where are the sugar radicals in irradiated DNA? *Radiat. Res.* **147**, 663–673 (1997).
17. M. Yan, D. Becker, S. Summerfield, P. Renke and M. D. Sevilla, Relative abundance and reactivity of primary ion radicals in γ-irradiated DNA at low temperatures. 2. Single- vs double-stranded DNA. *J. Phys. Chem.* **96**, 1983–1989 (1992).
18. B. Weiland, J. Hüttermann and J. van Tol, Primary free radical formation in randomly oriented DNA: EPR spectroscopy at 245 GHz. *Acta Chem. Scand.* **51**, 585–592 (1997).
19. M. D. Sevilla and D. Becker, Radiation Damage in DNA. In *Specialist Periodical Reports, Electron Spin Resonance* (M. M. Atherton, M. J. Davies and B. C. Gilbert, Eds.), pp. 130–165. Royal Society of Chemistry, Cambridge, 1994.
20. M. D. Sevilla and D. Becker, Radiation damage to DNA and related biomolecules. In *Specialist Periodical Reports, Electron Spin Resonance* (M. M. Atherton, M. J. Davies and B. C. Gilbert, Eds.), pp. 79–115. Royal Society of Chemistry, Cambridge, 1997.
21. N. J. Turro, *Molecular Photochemistry*, p. 224. W. A. Benjamin, Reading, MA, 1965.
22. G. Kraft and M. Kramer, Linear energy transfer and track structure. *Adv. Radiat. Biol.* **17**, 1–52 (1993).
23. J. J. Butts and R. Katz, Theory of RBE for heavy ion bombardment of dry enzymes and viruses. *Radiat. Res.* **30**, 885–871 (1967).
24. A. Chatterjee and W. R. Holley, Computer simulation of initial events in the biochemical mechanisms of DNA damage. *Adv. Radiat. Biol.* **17**, 181–226 (1993).
25. R. Katz, R. Zachariah, F. A. Cucinotta and C. Zhang, Survey of cellular radiosensitivity parameters. *Radiat. Res.* **140**, 356–365 (1994).
26. M. Scholz and G. Kraft, Calculation of heavy ion inactivation probabilities based on track structure, x ray sensitivity and target size. *Radiat. Prot. Dosim.* **52**, 29–33 (1994).
27. A. Chatterjee and J. L. Magee, Track models and radiation chemical yields. In *Radiation Chemistry, Principles and Applications* (Farhataziz and M. A. J. Rodgers, Eds.) pp 173–199. VCH Publishers, New York, 1987.
28. Z. Cai and M. D. Sevilla, Electron spin resonance study of electron transfer in DNA: Inter-double strand tunneling processes. *J. Phys. Chem. B* **104**, 6942–6949 (2000).
29. Z. Cai, Z. Gu and M. D. Sevilla, Electron spin resonance study of electron and hole transfer in DNA: The effects of hydration, aliphatic amine cations and histone proteins. *J. Phys. Chem. B* **105**, 6031–6041 (2001).
30. A. Schaefer, J. Hüttermann and G. Kraft, Free radicals from polycrystalline pyrimidines and purines upon heavy ion bombardment at low temperatures: An electron spin resonance study. *Int. J. Radiat. Biol.* **63**, 139–149 (1993).
31. S. G. Swarts, D. Becker, M. D. Sevilla and K. T. Wheeler, Radiation-induced DNA damage as a function of hydration. II. Base damage from electron loss centers. *Radiat. Res.* **145**, 304–314 (1996).
32. Y. Razskazovskiy, M. G. Debije and W. A. Bernhard, Direct radiation damage to crystalline DNA: What is the source of unaltered base release? *Radiat. Res.* **153**, 436–441 (2000).
33. C. Bienfait, J. Ceulemans and P. Claes, Radiation chemistry of n-pentane in the solid phase. In *Radiation Chemistry II* (R. Gould, Ed.), pp. 300–310. American Chemical Society, Washington, DC, 1968.
34. W. H. Hamill, Ionic processes in γ-irradiated solids at −196°. In *Radical Ions* (E. T. Kaiser and L. Kevan, Eds.), pp. 321–416. Interscience, New York, 1968.
35. S. Z. Toma and W. H. Hamill, The mechanism of hydrogen formation in the radiolysis of cyclohexane and other hydrocarbons. *J. Am. Chem. Soc.* **86** 1478–1483 (1964).
36. S. Z. Toma and W. H. Hamill, The mechanism of hydrogen formation in γ-irradiated hydrocarbons. *J. Am. Chem. Soc.* **86** 4761–4764 (1964).
37. C. M. L. Kerr, K. Webster and F. Williams, Electron spin resonance evidence for dissociative electron capture in γ-irradiated phosphate esters. *J. Phys. Chem.* **76**, 2848–2850 (1972).
38. D. Nelson and M. C. R. Symons, Unstable intermediates. Part 169. Electron capture processes in organic phosphates: an electron spin resonance study. *J. Chem. Soc. Perkin II*, 286–293 (1977).
39. D. J. Nelson, M. C. R. Symons and J. L. Wyatt, Electron paramagnetic resonance studies of irradiated D-glucose-6-phosphate ions: relevance to DNA. *J. Chem. Soc. Faraday Trans.* **89**, 1955–1958 (1993).
40. W. A. Bernhard and F. S. Ezra, Electron spin resonance of γ-irradi-

ated alkyl phosphates: The C_2H_5 radical in magnesium diethyl phosphate. *J. Chem. Phys.* **60**, 1707–1710 (1974).

41. A. Sanderud and E. Sagstuen, EPR study of x-irradiated hydroxylalkyl phosphate esters. Phosphate radical formation in polycrystalline glucose phosphate, ribose phosphate and glycerol phosphate salts at 77 K and 295 K. *J. Chem. Soc. Faraday Trans.* **92**, 995–999 (1996).

42. C. Von Sonntag, *The Chemical Basis of Radiation Biology*. Taylor & Francis, London, 1987.

43. P. O'Neill and E. M. Fielden, Free radical processes in DNA. *Adv. Radiat. Biol.* **17**, 53–120 (1993).

44. B. Boudaïffa, P. Cloutier, D. Hunting, M. A. Huels and L. Sanche, Cross sections for low energy (10–50 eV) electron damage to DNA. *Radiat. Res.* **157**, 227–234 (2002).

45. H. Abdoul-Carime and L. Sanche, Sequence-specific damage induced by the impact of 3–30 eV electrons on oligonucleotides. *Radiat. Res.* **156**, 151–157 (2001).

46. B. Boudaïffa, P. Cloutier, D. Hunting, M. A. Huels, and L. Sanche, Resonant formation of DNA strand breaks by low-energy (3–30 eV) electrons. *Science* **287**, 1658–1660 (2000).